18

Highly-directive polymeric quasicrystalline antenna

© A.A. Chuev[1], V.A. Chistyakov[1,¶], A.A. Dudnikova[1], A.D. Sayanskiy[1], M.S. Sidorenko[1], M.V. Rybin[1,2]

[1] ITMO University, Physics Faculty, St. Petersburg, Russia
[2] Ioffe Institute, St. Petersburg, Russia

¶e-mail: v.chistyakov@metalab.ifmo.ru

Received April 22, 2025
Revised April 28, 2025
Accepted April 29, 2025

The development of optical antennas is a critical challenge in modern photonics. Contemporary technological capabilities for fabricating such elements impose several constraints, including planar modulation of dielectric permittivity. Additionally, it is desirable to use low-absorption materials with a low refractive index. This study presents the results of the design and investigation of dielectric nanoantennas based on low-contrast quasicrystalline structures, which enable the formation of a radiation pattern from a dipole source. The material distribution within the structure is determined using an inverse design method and computational optimization to achieve the maximum gain coefficient. Theoretical analysis of the optimized optical antenna properties demonstrates a radiation gain of up to 10 dBi when using materials with a refractive index of 1.48.

Keywords: quasicrystalline photonic structure, inverse design method, optical antennas, high directivity, low-refractive-index materials.

DOI: 10.61011/EOS.2025.07.61907.7861-25

Introduction

Recent decades have witnessed rapid development in the study of artificial media for electromagnetic field control, such as photonic crystals (PCs) and metamaterials composed of artificial meta-atoms with resonant properties [1]. In PCs, the refractive index distribution exhibits periodic modulation resulting in allowed and forbidden states [2]. Special interest lies in the band structure analysis, as it opens applied possibilities for controlling spontaneous emission in nanoscale photonic devices. In most cases, optical emission is due to electronic dipole transitions, the probability of which depends not only on the matrix element but also on the local density of photonic states (LDOS), known as the Purcell effect. At frequencies corresponding to the photonic bandgap, there are no electromagnetic field states, so electronic emission transitions do not occur. In contrast, near bandgap edges, the LDOS values are high, accelerating emission by increasing the electronic transition probability. Remarkably, the LDOS is defined not only for periodic structures but also for arbitrary dielectric environments surrounding the emitter. This opens prospects for creating efficient nanoantennas, i.e., optical-range antennas. A nanoantenna converts strongly localized electromagnetic fields created by a dipole source into electromagnetic waves in free space and vice versa. Since the 2010s, active research has been published on nanoantenna design and practical implementation due to progress in 3D nanotechnologies [3–5]. Nanoantennas find applications in biosensing [6], spectroscopy [7], optical trapping [8], and optical computing [9]. Additionally, they are crucial in prospective quantum data transmission systems requiring efficient transfer of optical signals between parts of quantum transmission lines [9].

Typically, nanoantenna design is based on known radio physics configurations and intuitive considerations. An alternative approach is inverse design methods employing numerical optimization [10,11]. These methods lead to complex material distributions but demonstrate higher performance compared to occasional analogs. Most inverse design techniques define target electromagnetic device properties, after which an algorithm finds a structure meeting those requirements. This somewhat resembles holography methods [12]. Recently [13,14], quasicrystalline structures based on reciprocal-space modification were reported, forming full photonic bandgaps in 2D and 3D media at low dielectric contrast. A similar approach enabled the development of optically transparent quasicrystalline structures with wavelength- and angle-dependent selective scattering [15,16]. These structures rely on multiple sinusoidal lattices with individual angular coordinates in reciprocal space. It is important to emphasize that, since the band structure of quasicrystalline systems can depend directly on lattice orientation, they can be optimized for high gain in optical antennas based on them.

In this work, we propose low-contrast nanoantennas based on quasicrystalline structures for enhancing dipole source emission at the stop-band edge wavelength (Fig. 1). The material distribution within the structure is found using an inverse design method. A set of lattices with random angular coordinates in reciprocal space is optimized to achieve maximum nanoantenna gain. Calculations are performed for structures made of material with a refractive index of 1.48, corresponding to available materials (silicon dioxide, polymers, etc.). As a result of optimization, the

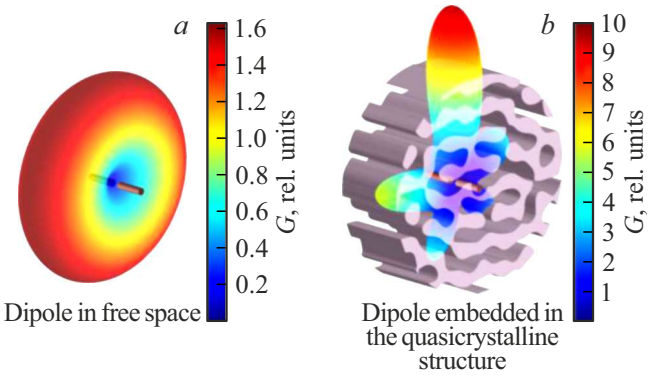

Figure 1. (*a*) Radiation pattern of an elementary dipole. (*b*) Radiation pattern of an elementary dipole embedded in the center of a quasicrystalline structure. Emission wavelength is $\lambda = 1550$ nm.

focused emission gain of the nanoantenna exceeds twice that of the pre-optimization structure.

Structure Design

A quasicrystalline photonic structure is formed by the Fourier transform of maxima (delta-like peaks) arranged on a circle in reciprocal space with individual angular coordinates but equal amplitude and phase. In direct space, the material distribution of the formed structure will have a continuous refractive index. For experimental feasibility, the photonic structure is binarized, producing a structure made of two materials with different refractive indices. Mathematically, the binary refractive index distribution can be represented as follows:

$$n_b(\mathbf{r}) = \Theta\left\{\sum_{i=1}^{N} \sin(\mathbf{k}_i \cdot \mathbf{r})\right\}, \qquad (1)$$

where Θ is the Heaviside function, N is the total number of maxima on the reciprocal space circle, $\mathbf{k}_i$ is the direction to the maximum with index i. Note that two maxima are actually used because the Fourier transform of a sinusoidal function corresponds to two delta-like peaks with coordinates $\pm\mathbf{k}_{ij}$ in reciprocal space. Each lattice has the same period $a = 526$ nm, so the distance from the circle center to each maximum is $|\mathbf{k}_i| = k_0 = 2\pi/a$. Fig. 2, *a* shows the distribution of ten lattices on a circle in reciprocal space with random angular coordinates α_i.

In the equation above, the Heaviside function defines the binarization procedure. The binary refractive index distribution $n_b(\mathbf{r})$ will be zero for negative Fourier transform values and one for positive values. Let zero correspond to air refractive index $n_1 = 1$. Ones represent material $n_2 = 1.48$, characteristic of widely available dielectrics such as polymers or silicon dioxide. Additionally, it is assumed the material has low absorption $\tan\delta = 0.001$. Note that the binarization results in a filling factor of 50% for both materials.

Because the emission pattern of a dipole source (Fig. 1,*a*) has a toroidal shape, we restrict the refractive index distribution in direct space within a disk shape of base diameter $L = 8a$ and height $h = 2a$. Fig. 2, *b* shows an example of such a structure based on randomly distributed angular lattice coordinates in reciprocal space.

Structure Optimization

Numerical modeling presented in this work was performed using the commercial software *CST Studio Suite*. An elementary dipole oriented along the *z*-axis was placed at the center of the quasicrystalline structure (Fig. 2, *b*). The source was surrounded directly by air filling a small cylindrical space. The variation in dipole radiation characteristics is due to the change in LDOS. Note that a significant increase in LDOS was previously observed at the edges of 1D PC stop-bands [17]. This effect is explained by the reduced modal group velocity $\delta\omega/\delta k$ near stop-band edges compared to free space modal group velocity, leading to enhanced LDOS at the emitter location [18]. The increase in the LDOS can be found from the power radiated by the dipole, P knowing the real part of the radiation impedance [19]. The obtained value is normalized by the radiation of a dipole P_0 in a homogeneous medium with the average refractive index of the structure. Fig. 3, *c* shows the normalized power spectrum of the dipole radiation for a random distribution of lattice directions in the quasicrystalline structure. The spectrum demonstrates a band of radiation suppression (photonic bandgap) around the wavelength of 1370 nm. For the telecommunications wavelength $\lambda = 1550$ nm an enhancement of the radiated power compared to the homogeneous medium is observed. It is known that in the far field of the dipole radiation, the electric and magnetic field vectors are in phase. Therefore, efficient energy transfer to the far field is expected at the wavelength of 1550 nm [20].

An important characteristic of nanoantennas is the radiation directivity, i.e., the gain of transmitted and received power in a specific direction. The radiation directivity is characterized by the directivity coefficient (DC): $D(\theta, \phi) = 4\pi P(\theta, \phi)/P_{tot}$, where $P(\theta, \phi)$ is the radiated power density in the direction of spherical angular coordinates (θ, ϕ), P_{tot} is the total radiated power in all directions. A parameter that takes into account losses in the materials forming the quasicrystalline structure is the gain coefficient (GC) G, which is unambiguously related to the DC $G = \eta D$, where $0 \leq \eta < 1$ is the efficiency factor. Fig. 2, *d* shows the three-dimensional radiation pattern of a dipole located at the center of the quasicrystalline structure at the wavelength 1550 nm. The non-optimized optical antenna exhibits a maximum GC of $G_0 = 5.25$ dBi and a main lobe width of 43°. It is generally accepted that highly directional antennas have a main lobe beamwidth of several

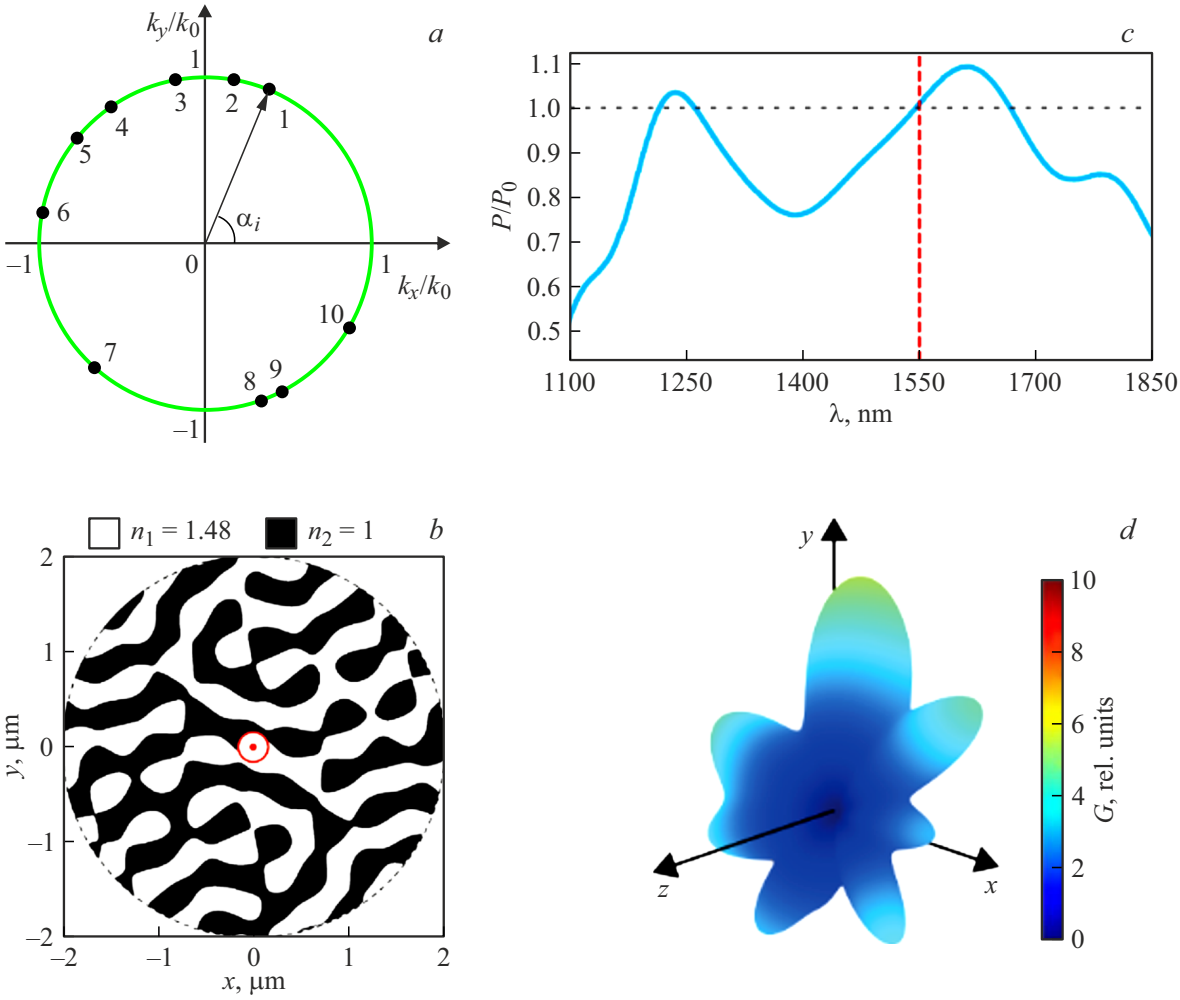

Figure 2. (*a*) Schematic representation of ten maxima in reciprocal space with random angular lattice coordinates α_i. (*b*) Image of the generated quasicrystalline structure based on random angular lattice coordinates. (*c*) Normalized power spectrum of emission of an elementary dipole embedded in the center of the quasicrystalline structure. (*d*) Radiation pattern of an elementary dipole embedded in the center of the quasicrystalline structure. Emission wavelength is $\lambda = 1550$ nm.

degrees ($5 - 20°$), and a GC of about 10 dBi. Thus, the non-optimized quasicrystalline antenna system is not highly directional.

Nanoantenna Optimization

The main goal of the optimization was to determine the geometry of the quasicrystalline nanoantenna that provides high directivity of the dipole source emission in a selected direction. To do this, a two-stage optimization procedure was applied. At the first stage, an iterative Bayesian algorithm [21] was used, based on the search for minima of a function with an a priori unknown number of local extrema. The geometry of the structure, the maximum GC G_0 and direction of gain depend on the polar coordinates of the lattices α_i. Thus, the mathematical formulation of the problem reduces to the search for the global maximum G_m of the objective function of our system $G_0(\alpha_i)$, i.e., maximizing the GC G_0 by varying the polar coordinates of the lattices:

$$G_m = \max_{0 \le \alpha_i \le 2\pi} G_0(\alpha_i). \quad (2)$$

Bayesian optimization uses a probabilistic model based on Gaussian processes to predict the objective function values at points where it has not yet been evaluated. The advantage of this approach is its efficiency in optimizing resource-intensive functions that require significant computational effort. At each optimization step, the algorithm constructs a probabilistic interpolation of the objective function between its known values corresponding to α_i sets obtained at previous iterations. A Gaussian process models the prior distribution and determines a utility function based on which the most probable values in the α_i parameter set are chosen for the next iteration step. Thus, Bayesian optimization minimizes the number of objective function evaluations but increases the mathematical complexity of determining the

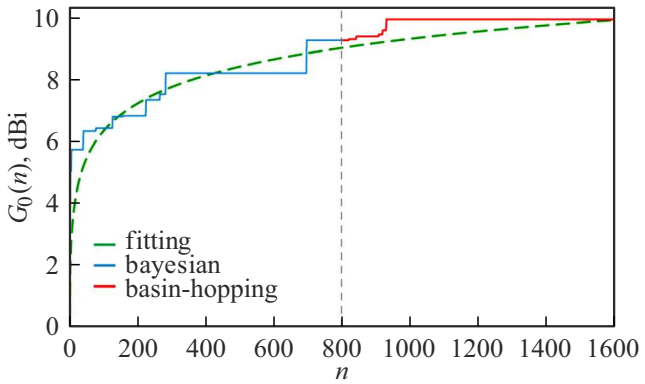

Figure 3. Graph of the maximum gain coefficient dependence on iteration number obtained by Bayesian optimization method (blue line) and local-jump optimization (red line). The green dashed line shows the approximation function. The inset shows convergence curve in logarithmic scale.

next step as the problem's dimensionality grows. Therefore, at some point, Bayesian optimization becomes less effective than other methods.

On the first iteration, a randomly generated set of angular coordinatesα_i (Fig. 2, *a*) was used. Calculation of the far-field radiation pattern was performed at the wavelength $\lambda = 1550$ nm. At each iteration, the Bayesian optimization algorithm calculates the objective function and adjusts the polar coordinate values α_i to improve the expected objective function value at the next step.

The computation time for the objective function was approximately 40 s using our computational resources. The execution time of the initial iterations was comparable to the objective function evaluation time, but increased as the number of iterations grew. The Bayesian optimization process was stopped after 800 iterations since one iteration took about an hour. Figure 3 shows in blue the dependence of the maximum GC on the iteration number obtained by Bayesian optimization. The GC maximum increases with iteration number and tends toward 10 dBi. Visually, the graph reaches a plateau at $G_0 = 9.24$ dBi. The inset shows the convergence curve of the GC maximum versus iteration number on a logarithmic scale. The presented dependence is linear and can be approximated by the logarithmic function $G_0(n) \approx 3lg(n+1) + 0.3$, where n is the iteration number. The approximation function is shown by a green dashed line, which describes the convergence curve well.

Next, to refine the quasicrystalline structure design after the Bayesian algorithm, we used the local-jump optimization method (*basin-hopping*) [22]. This algorithm combines two key approaches: random perturbation of system parameters followed by local optimization and a probabilistic acceptance criterion for new α_i sets. The initial iteration used the angular coordinates obtained from Bayesian optimization. We expected to further improve on the results from the previous stage.

In Figure 3, the red line shows the dependence of the maximum GC on iteration number obtained by local-jump optimization. The study included 800 iterations with 40 seconds computation time per iteration. As a result, the GC was maximized to $G_0 = 9.92$ dBi. The observed dependence is well described by the previously proposed approximation function (green dashed line).

We analyzed the geometry of the optimized structure obtained by the local-jump algorithm. Optimization results for lattice polar coordinates are presented in Fig. 4, *a*. Most maxima on the circle are concentrated at the pole in the positive direction of the k_y axis. The geometry of the optimized quasicrystalline antenna in direct space is shown in Fig. 4, *b*. Visually, the material distribution resembles a Bragg lattice with alternating layers along the y-axis. The normalized emission power spectrum P/P_0 in Fig. 4, *c* shows a maximum near the wavelength 1620 nm. Although the LDOS peak is shifted relative to the expected wavelength of 1550 nm, the emission power enhancement effect manifests in a narrow band around the LDOS peak. Fig. 4, *d* shows the three-dimensional radiation pattern of the considered structure at 1550,nm wavelength. The main lobe is primarily directed along the positive y-axis direction, and the emission intensity in the opposite direction is significantly suppressed. The main lobe width is 20°, and the GC maximum reaches $G_0 = 9.92$ dBi. From this, it can be concluded that the optimized quasicrystalline structure realizes a highly directional nanoantenna mode with specified characteristics.

Discussion of Results

Since the design in reciprocal space is unrestricted (unlike periodic photonic analogs), the characteristics of the proposed antenna system can be modified. Using optimization methods, we can shape focused emission of the embedded dipole source toward more than one direction. Compared to highly directional plasmonic antennas, our design exhibits significantly lower dissipative losses ($\tan\delta \approx 10^{-3}$) due to the use of a dielectric material with low refractive index contrast and elimination of resistive loads. Modern electron-beam lithography techniques make it possible to fabricate the proposed structure with nanometer precision from available optically transparent polymers. The use of low-contrast dielectric materials in the design of our antenna also offers advantages over nanoantennas with high dielectric permittivity in optical information transmission systems, as they exhibit a low reflection coefficient when receiving signals.

Conclusion

Thus, we have demonstrated a dielectric nanoantenna based on a quasicrystalline structure with a low material contrast of 1.48, designed using the inverse design method in reciprocal space. In reciprocal space, the random

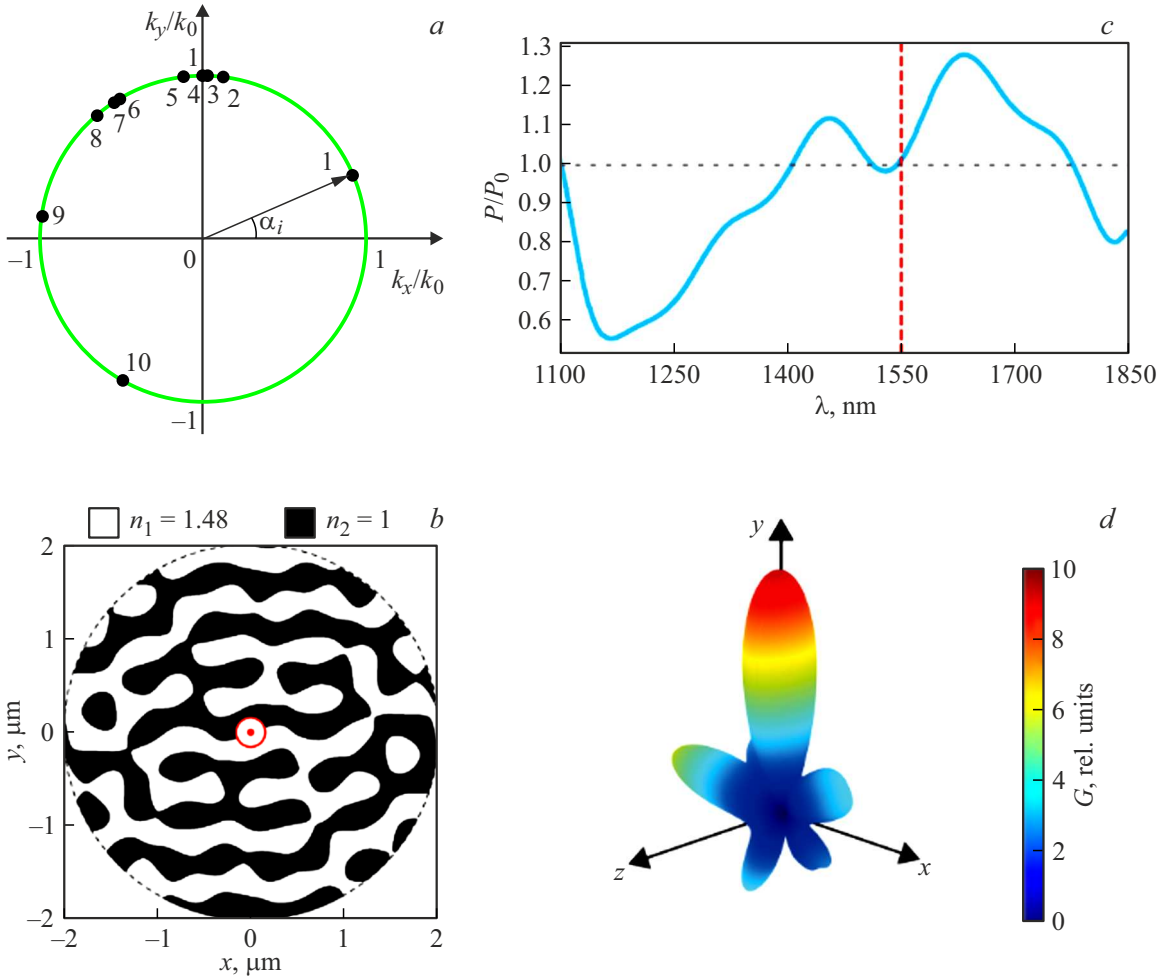

Figure 4. (*a*) Schematic representation of ten maxima in reciprocal space with lattice angular coordinates α_i obtained by optimization. (*b*) Image of the generated quasicrystalline structure based on optimized angular lattice coordinates. (*c*) Normalized power spectrum of emission of an elementary dipole embedded in the center of the quasicrystalline structure. (*d*) Radiation pattern of an elementary dipole embedded in the center of the quasicrystalline structure. Emission wavelength is $\lambda = 1550$ nm.

distribution of maxima along the circle corresponds to a set of lattices in direct space. To achieve directional enhancement of the embedded dipole source, we optimized the random angular coordinates of the lattices. Focused emission enhancement in such a structure is observed near the boundary frequency of the stop-band. We showed that the gain coefficient reaches 10 dBi in the optimized structure. Antennas of this type may find application in optical information transmission and computing systems.

Funding

This work was supported by the Russian Science Foundation (grant 20-79-10316).

Conflict of interest

The authors declare that they have no conflict of interest.

References

[1] M.V. Rybin, M.F. Limonov, UFN, bf 189, 881 (2019). (in Russian)
[2] J.D. Joannopoulos, S.G. Johnson, J.N. Winn, R.D. Meade. *Photonic Crystals: Molding the Flow of Light* (Princeton University Press, Princeton, 2008), 2nd edn.
[3] A.F. Koenderink. ACS Photonics, **4**, 710 (2017).
[4] M.R. Hasan, O.G. Hellesø. Nanotechnology, **32**, 202001 (2021).
[5] N. Li, Y. Lai, S.H. Lam, H. Bai, L. Shao, J. Wang. Advanced Optical Materials, **9**, 2001081 (2021).
[6] A. Tittl, C. Kremers, J. Dorfmuller, D.N. Chigrin, H. Giessen. Optical Materials Express, **2**, 111 (2012).
[7] F. Neubrech, C. Huck, K. Weber, A. Pucci, H. Giessen. Chemical Reviews, **117**, 5110 (2017).
[8] B.J. Roxworthy, K.D. Ko, A. Kumar, K.H. Fung, E.K. Chow, G.L. Liu, N.X. Fang, K.C. Toussaint, Jr. Nano Letters, **12**, 796 (2012).
[9] A. Alu, N. Engheta. Physical Review Letters, **104**, 213902 (2010).

[10] P.R. Wiecha, A. Arbouet, C. Girard, O.L. Muskens. Photonics Research, **9**, B182 (2021).
[11] R. Hernandez, P.R. Wiecha, J.M. Poumirol, G. Agez, A. Arbouet, L. Ressier, V. Paillard, A. Cuche. JOSA B, **41**, A108 (2024).
[12] H. Wang, W. Jin, C. Guo, N. Zhao, S.P. Rodrigues, S. Fan. ACS Photonics, **9**, 1358 (2022).
[13] L. Maiwald, T. Sommer, M.S. Sidorenko, R.R. Yafyasov, M.E. Mustafa, M. Schulz, M.V. Rybin, M. Eich, A.Y. Petrov. Advanced optical materials, **10**, 2100785 (2022).
[14] V.A. Chistyakov, R.R. Yafyasov, A.D. Sayanskiy, M.S. Sidorenko, M.V. Rybin. Opt. Lett., **49**, 3664 (2024).
[15] V.A. Chistyakov, M.S. Sidorenko, A.D. Sayanskiy, M.V. Rybin. JETP Letters, **117**, 742 (2023).
[16] M.E. Mustafa, M. Eich, A.Y. Petrov. Opt. Mater. Express, **14**, 1281 (2024).
[17] J.P. Dowling, M. Scalora, M.J. Bloemer, C.M. Bowden. J. Applied Physics, **75**, 1896 (1994).
[18] K. Sakoda. *Optical properties of photonic crystals*, vol. 2, (Springer, 2005).
[19] A.E. Krasnok, A.P. Slobozhanyuk, C.R. Simovski, S.A. Tretyakov, A.N. Poddubny, A.E. Miroshnichenko, Y.S. Kivshar, P.A. Belov. Scientific Reports, **5**, 12956 (2015).
[20] B.B. Nikol'skij.
it Elektrodinamika i rasprostranenie radiovoln [Ucheb. posobie dlya radiotekhn. spec. vuzov], (Nauka, Moskva, 1989). (in Russian)
[21] P.I. Frazier. arXiv preprint arXiv:1807.02811 (2018).
[22] D.J. Wales, J.P. Doye. J. Physical Chemistry A, **101**, 5111 (1997).

Translated by J.Savelyeva